PHASE FIELD MODELING OF EQUILIBRIUM SHAPES AND GROWTH MORPHOLOGIES IN Al-Zn ALLOYS

Jonathan Friedli[1], Aurèle Mariaux[1], Frédéric Gonzales[1], Michel Rappaz[1]

[1]Computational Materials Laboratory, Ecole Polytechnique Fédérale de Lausanne, CH-1015 Lausanne, Switzerland

Keywords: Interfacial Energy Anisotropy, Phase Field, Curvature, Stiffness

Abstract

The anisotropy of the solid-liquid interfacial energy, γ_{sl}, plays a key role in the accurate prediction of growth morphologies in metallic alloys. This interfacial energy anisotropy can vary due to alloy composition, especially when that of the pure solvent is weak. Recently Gonzales and Rappaz [1] showed the influence of an increasing zinc content on the growth direction of aluminum dendrites, which varied progressively from $\langle 100 \rangle$ to $\langle 110 \rangle$ as the zinc composition changed from 10 to 90 wt%. At the onset and end of this dendrite orientation transition (DOT), textured seaweeds were even observed. While this DOT could be simulated by phase field modeling with a change in the anisotropy of γ_{sl}, seaweed could not be reproduced [2]. In order to explain this disagreement, it is necessary to have direct access to the anisotropy parameters. A combined numerical/experimental methodology to determine the needed experimental data is presented. It is based on inverse methods applied to 3D equilibrium shapes obtained by X-ray tomography. The gained anisotropy values are evaluated in a phase field code featuring a description of the interfacial energy anisotropy by a development up to the third order of the spherical harmonics for a cubic system. The latter enables to model growth directions out of $\{110\}$ planes, which was not possible with previous models.

Introduction

Although aluminum has been produced commercially for more than 100 years with an annual production exceeding 30 millions tons in 2007, many fundamental questions regarding its solidification remain. For example, Gonzales and Rappaz [1] have recently shown that an increase in the zinc content of Al-Zn alloys continuously changes the dendrite growth direction from $\langle 100 \rangle$ to $\langle 110 \rangle$ in a $\{110\}$ plane (Fig. 1). At intermediate compositions (around 50 wt%), $\langle 320 \rangle$ dendrites were observed, whereas at the onset and end of this so-called "Dendrite Orientation Transition" (DOT), textured seaweeds grew with an average orientation following the master curve of Fig. 1. Since these solidification experiments were conducted at low to moderate growth rate, the contribution of attachment kinetics can be discarded. Therefore, these variations of growth morphologies/directions were attributed to the influence of zinc on the weak anisotropy of the solid-liquid interfacial energy γ_{sl} of aluminum. Introducing a variable anisotropy in γ_{sl}, phase field simulations could reproduce this DOT from $\langle 100 \rangle$ to $\langle 110 \rangle$, even with $\langle 320 \rangle$ dendrites, but not the textured seaweeds [2].

It is commonly stated in most solidification textbooks that dendrites in cubic metals grow along $\langle 100 \rangle$ directions, since these directions correspond to maxima of γ_{sl}. This is true in some cases when the anisotropy of γ_{sl} is strong, e.g., for nickel-base alloys, but not always. Furthermore, this statement is incorrect and it is more precise to say that dendrites grow from the most highly curved parts of the equilibrium crystal shape. As we shall recall

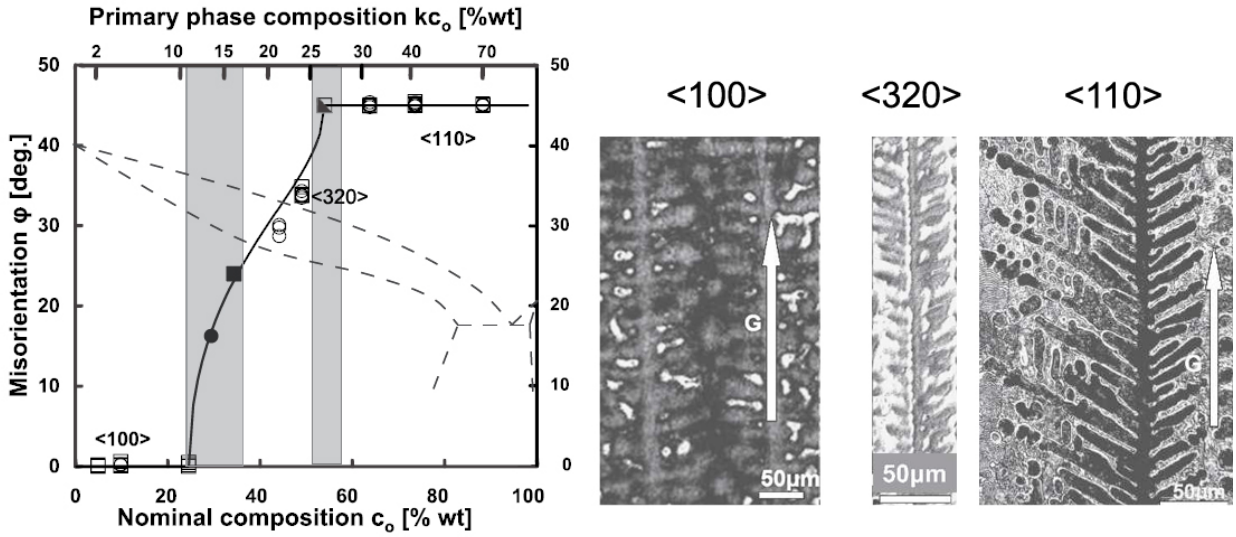

Figure 1: Left: Misorientation between the <hk0> direction of dendrites (open symbols) or of the main seaweed texture (filled symbols) and the ⟨100⟩ direction, as a function of the zinc concentration [1]. The corresponding Al-Zn phase diagram is superimposed with dashed lines on an arbitrary vertical scale for temperature. Right: longitudinal sections of Al-Zn specimens showing ⟨100⟩, ⟨320⟩ and ⟨110⟩ dendrites for a zinc composition of 10, 50 and 90 wt%, respectively.

in this work, these regions correspond to minima of the so-called solid-liquid interfacial "stiffness". In simple cases, maxima of γ_{sl} indeed correspond to minima of the stiffness, but not always [2]. Additionally, the problem gets more complicated when the two principal radii of curvature are not maximized at a single location of the equilibrium shape crystal. Therefore, a generally valid theory predicting dendrite growth directions in three dimensions for complex expressions of γ_{sl} is still lacking. In order to further analyze this problem and the DOT observed by Gonzales and Rappaz, quantitative measurements of the interfacial energy anisotropy in Al-Zn alloys are necessary.

One of the methodologies used to measure the interfacial energy anisotropy precisely consists in observing the shape of small crystals in equilibrium with the liquid phase, or conversely the shape of liquid droplets in equilibrium with the solid. With the help of mathematical tools such as the $\vec{\xi}$-vector formalism and the development of γ_{sl} into spherical harmonics compatible with the cubic symmetry, such shapes can be used to deduce the anisotropy of γ_{sl}. These values can then be introduced into phase field simulations for the prediction of growth morphologies under variable conditions. Ultimately, such correlations should allow establishing a more general theory of dendrite growth directions when the γ_{sl}-plot or stiffness-plot exhibit a complex shape.

The goal of this contribution is to describe the mathematical tools underlying this important solidification issue. The $\vec{\xi}$-vector formalism as well as curvature and stiffness calculations will be presented together with preliminary phase field simulations.

Theory

Interfacial energy anisotropy

The interfacial energy $\gamma_{sl}(n_x, n_y, n_z)$ can be described by a linear combination of spherical harmonics, themselves functions of the components (n_x, n_y, n_z) of the unit normal $\vec{n}$. Fol-

lowing Fehlner and Vosko [3], the development of γ_{sl} for a cubic symmetry crystal can be written as

$$\gamma_{sl}(\vec{n}) = \gamma_{sl}^0 \left[1 + \epsilon_1 \left(Q - \frac{3}{5} \right) + \epsilon_2 \left(3Q + 66S - \frac{17}{7} \right) + \epsilon_3 \left(65Q^2 - 94Q - 208S - 33 \right) + \ldots \right] \quad (1)$$

where $Q = n_x^4 + n_y^4 + n_z^4$, $S = n_x^2 n_y^2 n_z^2$, γ_{sl}^0 is a pre-factor and the ε_i's are the anisotropy parameters. For $\varepsilon_1 > 0$ and $\varepsilon_2 = \varepsilon_3 = 0$, $\langle 100 \rangle$ dendrites are obtained, whereas the case $\varepsilon_2 < 0$ and $\varepsilon_1 = \varepsilon_3 = 0$ corresponds to $\langle 110 \rangle$ dendrites. The so-called γ_{sl}-plot is simply given by $\gamma_{sl}(\vec{n})\vec{n}$.

$\vec{\xi}$-vector formalism

When a crystal is in equilibrium with a liquid (or vapor) phase, free from any contact or body forces, Wulff's theorem [4] states that the distance $d(\vec{n})$, projection on the normal $\vec{n}$ of the vector from the gravity center to the point on the surface with a normal $\vec{n}$ (see Fig. 2), is proportional to the corresponding free energy per unit area, $\gamma_{sl}(\vec{n})$. In other words, $d(\vec{n})/\gamma_{sl}(\vec{n})$ is constant. The proposed geometrical construction, the Wulff-plot, is equivalent to the so-called $\vec{\xi}$-plot, as demonstrated by Hoffman and Cahn [5]. The $\vec{\xi}$-vector is defined as $\vec{\xi}(\vec{n}) = \vec{\nabla}(r\gamma_{sl}(\vec{n}))$ and describes the equilibrium shape up to a scaling factor. If equation (1) is used for γ_{sl}, this formalism is then a very effective tool to go back and forth between the equilibrium shape and the γ_{sl}-plot ($\gamma_{sl}(\vec{n})\vec{n}$). Please note that, by construction, a given direction $\vec{n}$ does not correspond to the normal to the γ_{sl}-plot at point $\gamma_{sl}(\vec{n})\vec{n}$, but is parallel to the normal to the $\vec{\xi}$-plot at point $\vec{\xi}(\vec{n})$ [5].

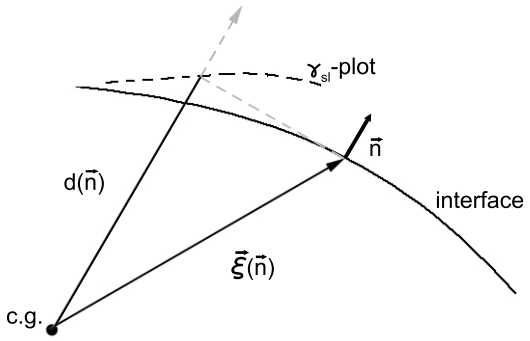

Figure 2: Schematic representation of the reverse Wulff construction for determining the γ_{sl}-plot starting from the equilibrium shape. c.g. is the center of gravity of the equilibrium shape.

Curvature

For simple cases where γ_{sl} is function of ε_1 only, convexities of the equilibrium shape are such that the two principal radii of curvature (or principal curvatures) of the equilibrium shape are minimum (maximum) and equal along $\langle 100 \rangle$. In this case, the growth directions are straightforward. However when the development of γ_{sl} goes up to the second order or more, this is no longer the case and the principal curvatures might not be maximum and equal along a given direction $\vec{n}$. (Please note that "a" direction $\vec{n}$ means all the equivalent

directions $\vec{n}$ that respect the cubic symmetry, e.g., when $\vec{n} = (\frac{1}{\sqrt{2}}, \frac{1}{\sqrt{2}}, 0)$, this includes the twelve $\langle 110 \rangle$ directions). In such complex cases, it is therefore necessary to determine the gaussian (K), mean (H) and principal (K_1, K_2) curvatures of the equilibrium shape for any expression of γ_{sl}. This can be done using the following relationships [6]

$$K = \frac{eg - f^2}{EG - F^2} \qquad H = \frac{eG - 2fF + gE}{2(EG - F^2)} \qquad K_i = H \pm \sqrt{H^2 - K} \tag{2}$$

where E, F, G and e, f, g are the coefficients of the first, respectively second, fundamental forms of the equilibrium shape crystal surface. Taking into account the fact that $\vec{n}$ is normal to the $\vec{\xi}$-plot at point $\vec{\xi}(\vec{n})$, these expressions are given by

$$E = \frac{\partial \vec{\xi}}{\partial \theta} \cdot \frac{\partial \vec{\xi}}{\partial \theta} \qquad F = \frac{\partial \vec{\xi}}{\partial \theta} \cdot \frac{\partial \vec{\xi}}{\partial \phi} \qquad G = \frac{\partial \vec{\xi}}{\partial \phi} \cdot \frac{\partial \vec{\xi}}{\partial \phi} \tag{3}$$

$$e = -\frac{\partial \vec{\xi}}{\partial \theta} \cdot \frac{\partial \vec{n}}{\partial \theta} \qquad f = -\frac{1}{2}\left(\frac{\partial \vec{\xi}}{\partial \theta} \cdot \frac{\partial \vec{n}}{\partial \phi} + \frac{\partial \vec{\xi}}{\partial \phi} \cdot \frac{\partial \vec{n}}{\partial \theta}\right) \qquad g = -\frac{\partial \vec{\xi}}{\partial \phi} \cdot \frac{\partial \vec{n}}{\partial \phi} \tag{4}$$

where θ and ϕ are the polar and azimuthal angles of the spherical coordinate system, respectively.

Stiffness

Another way of looking at the dendrite growth direction changes observed in Al-Zn alloys is to consider the *stiffness* of the solid-liquid interface [2]. As the name indicates, the stiffness measures the variation of surface energy associated with a local deformation of a sphere. The lower the stiffness, the more easily the sphere can be made more convex at a given location. The definition of the interfacial stiffness originates from Herring's relation [7] giving the variation of the chemical potential μ associated with the surface energy:

$$\frac{\mu}{V^m} = K_1 \left[\gamma_{sl}(\vec{n}) + \frac{\partial^2 \gamma_{sl}(\vec{n})}{\partial n_1^2}\right] + K_2 \left[\gamma_{sl}(\vec{n}) + \frac{\partial^2 \gamma_{sl}(\vec{n})}{\partial n_2^2}\right] \tag{5}$$

where V^m is the molar volume and the second derivative of γ_{sl} are taken along the corresponding principal directions of curvature (n_1,n_2). Taking $K_1 = K_2$ for a sphere, the variations of chemical potential along the surface is directly proportional to the stiffness Φ_{sl}

$$\Phi_{sl}(\vec{n}) = \gamma_{sl}(\vec{n}) + \frac{1}{2}\left[\frac{\partial^2 \gamma_{sl}(\vec{n})}{\partial n_1^2} + \frac{\partial^2 \gamma_{sl}(\vec{n})}{\partial n_2^2}\right] \tag{6}$$

Conversely, for an equilibrium crystal shape, the chemical potential is constant along the surface and the regions where the mean curvature is the highest are approximately given by the minima of the stiffness, but not exactly. Indeed, in three dimensions the stiffness is actually not a scalar but a symmetric tensor [8]. It measures the variation of energy associated with curving a sphere along any arbitrary direction (this includes curving along one or two arbitrary axes). A more correct way to write Herring's relation would thus be [8]

$$\frac{\mu}{V^m} = \underline{\underline{K}} : \underline{\underline{\Phi}}_{sl} = \begin{bmatrix} K_1 & 0 \\ 0 & K_2 \end{bmatrix} : \begin{bmatrix} \gamma_{sl}(\vec{n}) + \frac{\partial^2 \gamma_{sl}(\vec{n})}{\partial n_1^2} & \frac{\partial^2 \gamma_{sl}(\vec{n})}{\partial n_1 \partial n_2} \\ \frac{\partial^2 \gamma_{sl}(\vec{n})}{\partial n_2 \partial n_1} & \gamma_{sl}(\vec{n}) + \frac{\partial^2 \gamma_{sl}(\vec{n})}{\partial n_2^2} \end{bmatrix} \tag{7}$$

where $A : B = A_{ij} B_{ij}$. Again, this expression must be constant for an equilibrium crystal shape.

Experimental

Equilibrium Shape Measurement

Since equilibration of solid particles in suspension in a melt is very difficult due to sedimentation and convection, equilibrium shapes are usually measured for liquid droplets trapped in a solid matrix. This technique, introduced by Basterfield et al. [9] and Miller et al. [10], has been largely improved by Liu et al. [11]. It features a directional solidification followed by a dual step heat treatment, the first one to homogenize the solute composition and the second to liquify the discontinuous eutectic phase into fine liquid droplets in equilibrium with the solid matrix. After quench, this leads to a controlled distribution of quenched liquid droplets, embedded in a single crystal matrix. As the matrix is a single crystal, it offers the advantage that only one experiment is necessary for the interfacial energy to be known in all crystallographic directions. The orientation of the single crystal is determined by Electron Back-Scattered Diffraction (EBSD) and the equilibrium shape is measured by serial sectioning or X-ray tomography. These data can then be fed into a least square fit on the $\vec{\xi}$-plot, thus giving ultimately a set of anisotropy parameters $(\varepsilon_1, \varepsilon_2, \varepsilon_3)$. However, this technique is very delicate, especially when the anisotropy of γ_{sl} is low as in aluminum alloys. Fig. 3 shows a cross-section of a quenched liquid droplet in equilibrium with the solid for an Al-82wt%Zn alloy. It clearly shows the very weak anisotropy of aluminum even at high zinc concentration. Further work is being done in this system to determine the anisotropy parameters.

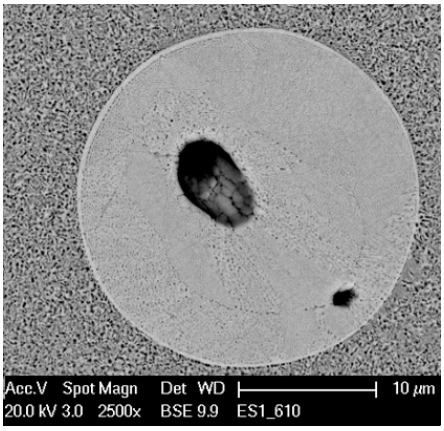

Figure 3: Section of an equilibrium shape in Al-82wt%Zn after 610 hours annealing at 392°C showing the very weak anisotropy in aluminum.

Modeling

Mathematica

Equations (1) to (7) have been implemented into a Mathematica® notebook, for an analytical analysis of the shape and curvature of equilibrium crystal shape. Due to the complexity of the equations, the stiffness tensor could not yet be evaluated, but the module already gives all the other parameters once $\gamma_{sl}(\vec{n})$ is specified ($\vec{\xi}$-plot Fig. 4(a), principal radii of curvature Fig. 4(c-d), mean and gaussian curvatures, etc.).

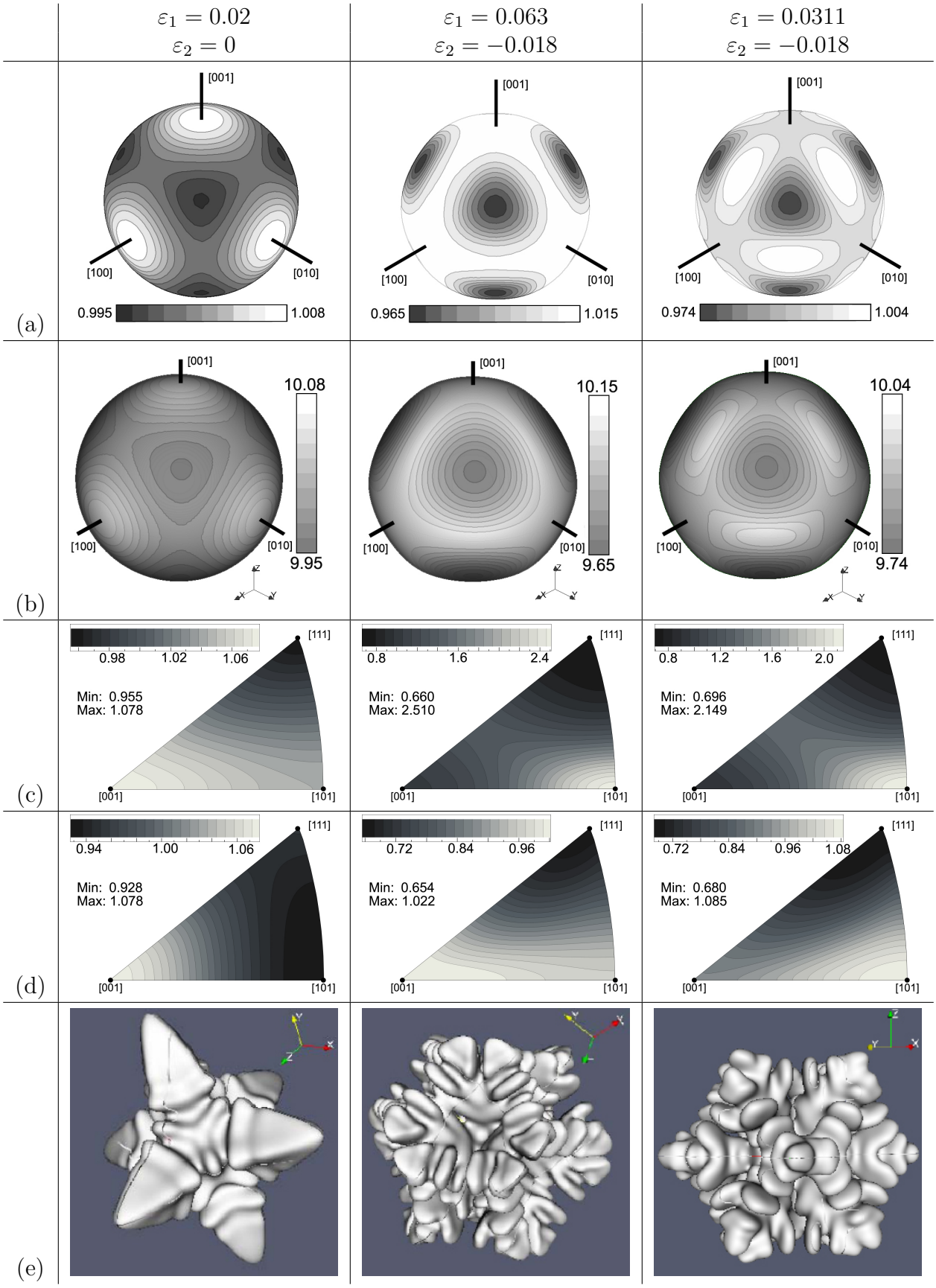

Figure 4: (a) Equilibrium shape, i.e. $\vec{\xi}$-plot, calculated by Mathematica®, (b) equilibrium shape obtained by phase field calculation, (c) first principal curvature, (d) second principal curvature, (e) $\langle 100 \rangle$, $\langle 320 \rangle$ and $\langle 110 \rangle$ equiaxed dendrites obtained by phase field calculation.

Phase Field

Phase field has been widely used for modeling dendrite growth and moving interface problems. The method used in the present study is similar to the phase field formulation by Tiaden et al. [12]. It is applied to 3 dimensional problems with equation (1) giving the anisotropy of the system. The model was run on a massively parallel computer for obtaining equilibrium shapes (Fig. 4(b)) and growth morphologies (Fig. 4(e)).

Equilibrium shape calculations were performed in a domain of $168 \times 168 \times 168$ cells, with a cell size of 0.1 μm and an initial sphere radius of 10 μm. To speed up the computations, advantage was taken of the symmetry of the crystal and only 1/8 of a sphere was modeled. Comparison between analytical equilibrium shapes and phase field computations shows a good agreement. Slight differences might be due to the mesh anisotropy in the phase field calculations, which has yet to be assessed and corrected.

Phase field calculations of dendrite growth were performed for domains made of $300 \times 300 \times 300$ cells with a cell size of 0.1 μm, an initial diameter of the nucleus of 1 μm, a fixed undercooling of 3 K and a cooling rate of -50 K/s. No advantage was taken of symmetries and the crystal orientation was taken off the grid axes to check the anisotropy introduced by the mesh.

In the first case ($\varepsilon_1 = 0.02$, $\varepsilon_2 = \varepsilon_3 = 0$) shown in Fig. 4, $\langle 100 \rangle$ dendrites are produced, whereas the last case ($\varepsilon_1 = 0.0311$, $\varepsilon_2 = -0.018$ and $\varepsilon_3 = 0$) corresponds to $\langle 110 \rangle$ dendrites. Analysis of the principal curvatures of the corresponding equilibrium shape crystal (Fig. 4(c-d)) indicates that in both cases the dendrites grow along the direction given by the maximum mean curvature, even when $\varepsilon_2 \neq 0$. However this is no longer the case for the intermediate situation shown in Fig. 4, where one of the two principal curvatures is maximum for $\langle 100 \rangle$ whereas the other one is maximum at $\langle 110 \rangle$ and for which $\langle 320 \rangle$ dendrite growth directions are observed. Indeed, neither the $\vec{\xi}$-plot convexities nor the curvature maxima are located along the $\langle 320 \rangle$ growth directions. These criteria thus fail to predict this growth direction which is nevertheless observed both in phase field simulations and experiments. Please note that this is an intermediate case, since one of the principal curvatures is maximum for $\langle 100 \rangle$ whereas the other is maximum at $\langle 110 \rangle$. The development of the stiffness tensor thus becomes absolutely necessary and might lead to a criterion which successfully predicts all types of growth directions.

Conclusion

All the necessary experimental techniques and mathematical tools for determining the interfacial energy anisotropy parameters and to evaluate its influence on equilibrium shape crystals and growth morphologies have been implemented. The first results show that equilibrium shape predictions based on the $\vec{\xi}$-vector formalism and phase field calculations are in good agreement. From the analytical formalism, the principal, mean and gaussian curvatures can be assessed. This should allow to correlate the observed equilibrium shape droplets with the anisotropy of the interfacial energy, and thus to compute growth morphologies using the phase field method. The present results show that the mean curvature can explain growth directions in the most simple cases, but is not the right criterion when higher orders of γ_{sl} are considered. In order to understand the detailed mechanisms of dendrite and seaweed growth in such cases, a full analysis of curvature and especially stiffness, over the whole range of anisotropy parameters, is necessary.

Acknowledgments

The authors gratefully acknowledge the financial support of the Fonds National Suisse pour la recherche scientifique (Grant No 200020-113260). They would like to thank also Jean-Luc Desbiolles for his invaluable help in building the massively parallel version of the phase field code. All electron microscopy measurements were obtained at the Centre Interdisciplinaire de Microscopie Electronique (CIME) at Ecole Polytechnique Fédérale de Lausanne (EPFL).

References

[1] F. Gonzales and M. Rappaz, "Dendrite growth directions in aluminum-zinc alloys", *Metallurgical and Materials Transactions A: Physical Metallurgy and Materials Science*, 37 (9) (2006), 2797–2806.

[2] T. Haxhimali, A. Karma, F. Gonzales, and M. Rappaz, "Orientation selection in dendritic evolution", *Nature Materials*, 5 (8) (2006), 660–664.

[3] W. R. Fehlner and S. H. Vosko, "Product representation for cubic harmonics and special directions for the determination of the fermi surface and related properties", *Canadian Journal of Physics*, 54 (21) (1976), 2159–2169.

[4] G. Wulff, "Zur Frage der Geschwindigkeit des Wachsthums und der Auflösung der Krystallflächen", *Zeitschrift für Kristallographie*, 34 (1901), 449–530.

[5] D.W. Hoffman and J.W. Cahn, "A vector thermodynamics for anisotropic surfaces. I. Fundamentals and application to plane surface junctions", *Surface Science*, 31 (C) (1972), 368–388.

[6] Alfred Gray. *Modern Differential Geometry of Curves and Surfaces with Mathematica*, chapter Surfaces In 3-Dimensional Space, 359–390. CRC Press, 2nd edition, 1999.

[7] C. Herring. *The physics of powder metallurgy*, chapter Surface tension as a motivation for sintering, 143–177. McGraw-Hill, 1951.

[8] D. Du, H. Zhang, and D.J. Srolovitz, "Properties and determination of the interface stiffness", *Acta Materialia*, 55 (2) (2007), 467–471.

[9] J. D. Basterfield, W. A. Miller, and G. C. Weatherly, "Anisotropy of interfacial free energy in solid-fluid and solid-solid system", *Canadian Metallurgy Quarterly*, 8 (1969), 131.

[10] W. A. Miller and G. A. Chadwick, "The equilibrium shapes of small liquid droplets in solid-liquid phase mixtures: Metallic h.c.p. and metalloid systems", *Proceedings of the Royal Society of London. Series A, Mathematical and Physical Science*, 312 (1509) (1969), 257–276.

[11] S. Liu, R. E. Napolitano, and R. Trivedi, "Measurement of anisotropy of crystal-melt interfacial energy for a binary Al-Cu alloy", *Acta Materialia*, 49 (20) (2001), 4271–4276.

[12] J. Tiaden, B. Nestler, H.J. Diepers, and I. Steinbach, "The multiphase-field model with an integrated concept for modelling solute diffusion", *Physica D: Nonlinear Phenomena*, 115 (1-2) (1998), 73–86.